Observation of bright exciton splitting in strained WSe$_2$ monolayers

A. Mitioglu,[1,2,3,*] J. Buhot,[1,2] M. V. Ballottin,[1,2] S. Anghel,[3,4] K. Sushkevich,[5] L. Kulyuk,[3] and P. C. M. Christianen[1,2,†]

[1]*High Field Magnet Laboratory (HFML - EMFL), Radboud University, 6525 ED Nijmegen, The Netherlands*
[2]*Institute for Molecules and Materials, Radboud University, 6525 AJ Nijmegen, The Netherlands*
[3]*Institute of Applied Physics, Academiei Str. 5, Chisinau, MD-2028, Republic of Moldova*
[4]*Experimentelle Physik 2, Technische Universität Dortmund, Otto-Hahn-Straße 4a, D-44227 Dortmund, Germany*
[5]*Moldova State University, Mateevici Str. 60, Chisinau, MD-2009, Republic of Moldova*

High-resolution magnetophotoluminescence measurements of strained WSe$_2$ monolayers are reported. At low temperature, a splitting of a few meV in the neutral exciton peak is observed, which is attributed to the theoretically predicted in-plane (*xy*) anisotropy splitting. Measurements in high magnetic fields up to 30 T demonstrate that strain and intervalley electron-hole exchange mix the valley-exciton energy levels, leading to a relaxation of the valley-selective optical selection rules and to strongly modified exciton *g* factors. Our observation of the bright exciton splitting provides crucial information about the dispersion of valley excitons and paves the way to develop valley functionality for photonic devices.

I. INTRODUCTION

Monolayers (MLs) of transition-metal dichalcogenides (TMDs), such as MoS$_2$, MoSe$_2$, WS$_2$, and WSe$_2$, are two-dimensional (2D) semiconductors with a honeycomb lattice, exhibiting direct band gaps in the K$^+$ and K$^-$ points at the corners of the hexagonal Brillouin zone [1–3]. Interestingly, these K$^+$ and K$^-$ valleys are not equivalent, but related to each other by time reversal. They can be individually addressed by respectively right- (σ^+) and left-handed (σ^-) circularly polarized light [Fig. 1(a)], because spin-orbit coupling and lack of inversion symmetry lift the spin degeneracy of the electron and hole states and lock the spin and valley (pseudospin) degrees of freedom [1]. Coulombic electron-hole (e-h) correlations are much stronger than in conventional semiconductor quantum wells, because of the 2D confinement, the reduced electric screening, and the relatively high carrier masses [3,4]. As a result, the optical spectra of ML TMDs are dominated by coupled electron-hole excitations (excitons) with binding energies as large as 0.5 eV [5]. ML TMDs form, therefore, a powerful platform to realize valleytronic materials in which stable valley excitons [2,5] and charged excitons (trions) can be created [6], exhibiting unique properties, such as valley polarization [7] and valley coherence [8], both of which can be tuned by external fields [9–13].

A common characteristic of low dimensional, direct band-gap semiconductor nanostructures is the importance of e-h exchange. Relative to bulk semiconductors, e-h exchange energies are enhanced in quasi-2D quantum wells [14,15] and (colloidal) quantum dots [16,17], up to values as large as 20 meV. Evidence for a finite e-h exchange has been found in ML TMDs, through an enhanced intervalley scattering rate [18], the absence of valley coherence for trions [4,8], and the

observation of inter- and intravalley trions [19,20]. Electron-hole exchange is, therefore, expected to be crucially important for all properties of tightly-bound excitons in ML TMDs [3,4,18,21]. For the bright K$^+$- and K$^-$-valley excitons two different contributions can be distinguished, the intra- (J_{intra}) and intervalley (J_{inter}) terms [Fig. 1(a)]. J_{inter} couples the two excitons in the opposite valleys, resulting in a splitting of the center-of-mass exciton dispersion into two branches. On each of these branches excitons have a linear polarization, with an in-plane projection that is either transversal (T) or longitudinal (L) to their 2D wave vector $K_{||}$ [Fig. 1(b), left panel]. Within the light cone ($K_{||} = 0$) the two branches are degenerate, whereas outside the light cone the L and T branches exhibit a splitting which increases with the $K_{||}$. This effect is similar to the longitudinal-transversal (L-T) splitting present in III-V quantum wells [14,15]. However, the TMD case is special because the exciton eigenstates are linear superpositions of two oppositely circularly polarized valley excitons, rather than of excitons of the same valley. The presence of uniaxial tensile strain breaks in-plane rotational symmetry, creating a finite J_{inter} at $K_{||} = 0$ that leads to a splitting Δ_0 between the exciton branches in the light cone [Fig. 1(b), right panel]. The splitting is wave-vector independent and is known as $K_{||} = 0$ *anisotropy splitting* [22–24]. Such a splitting opens up ways to coherently rotate the exciton valley pseudospin in a controllable manner. Thus, strained monolayer TMDs are a highly attractive system for studying optoelectronic applications, such as the exciton-based integrated photonic circuits. So far, observation of the bright exciton splitting in TMD MLs is lacking.

In this paper we investigate the energy fine structure of valley excitons in strained WSe$_2$ MLs. We detect Δ_0 by using low temperature (4.2 K), polarization-resolved, high-resolution microphotoluminescence (μ-PL) at zero applied magnetic field and we study the behavior of both exciton branches in fields up to 21 T. We have measured 7 WSe$_2$ ML flakes, mechanically exfoliated from different WSe$_2$ bulk

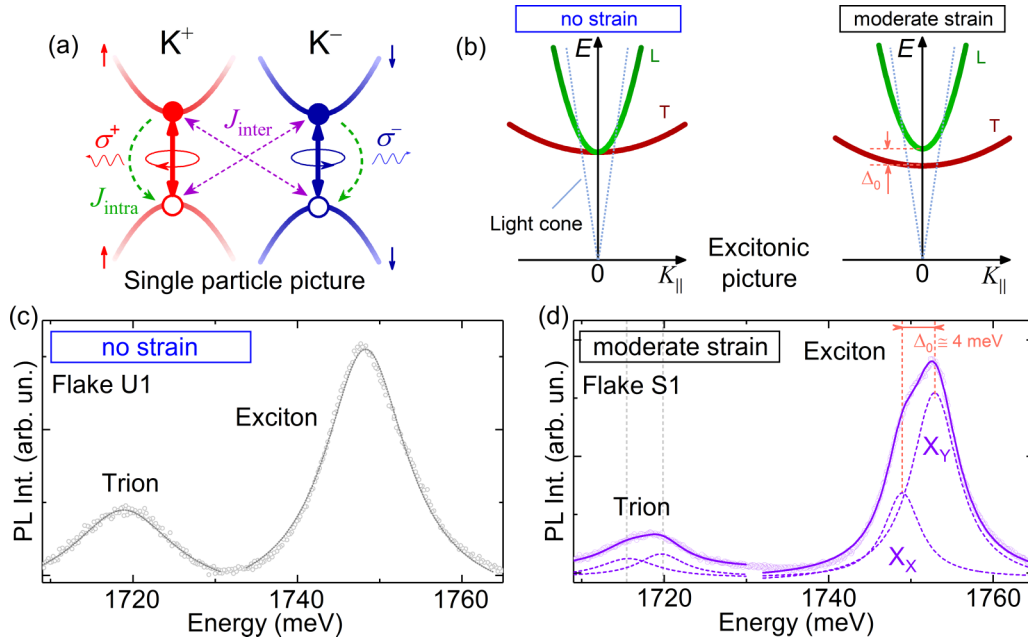*anatolie.mitioglu@ru.nl
†peter.christianen@ru.nl

FIG. 1. (a) Schematics of the conduction and valence bands (single particle picture) at the K^+ and K^- valleys of ML TMDs, showing the bright A-exciton transitions and the associated optical selection rules for σ^+ (red) and σ^- (blue) polarized light. Small arrows denote spin orientation. J_{intra} (dashed green arrows) and J_{inter} (dashed purple arrows) label the intra- and intervalley electron-hole (e-h) exchange interactions. (b) Valley-exciton dispersions in terms of the in-plane exciton center-of-mass wave vector $K_{||}$ (exciton picture). The bright exciton has two linearly polarized exchange-split branches associated with transversal (T) and longitudinal (L) excitons. The light cone (blue dashed lines) is the region where excitons (with energy E) can recombine radiatively ($K_{||} \leqslant E/\hbar c$, with $\hbar$ is the reduced Planck's constant and c the speed of light). Left panel: Without strain the two branches are degenerate at $K_{||} = 0$. Right panel: uniaxial tensile strain introduces a finite energy splitting (Δ_0) at $K_{||} = 0$. (c) Low temperature, unpolarized μ-PL spectra (symbols) of an unstrained WSe$_2$ ML (flake U1). The PL spectrum consists of two peaks, identified as the neutral A exciton and the negatively charged exciton (trion), which both can be fitted by Lorentzian lineshapes (solid lines). (d) Low temperature, unpolarized μ-PL spectrum (symbols) of a strained WSe$_2$ ML (flake S1). A splitting of both the neutral and charged exciton peaks is present. The dashed lines show the bi-Lorentzian fits to the doublet structures of the exciton and trion. The solid lines are the sum of these four peak functions. The excitons along x and y directions are labeled as X_X and X_Y, respectively. The fitted spectra are offset vertically for clarity.

crystals and deposited on Si/(90 nm) SiO$_2$ substrates (see Appendix, Materials and Methods section). We mainly describe PL and Raman spectra of two representative flakes (Flakes U1 and S1), where results of other flakes are given in the Appendix Secs. 1–4. The PL spectrum of a regular (unstrained) WSe$_2$ ML [Fig. 1(c)] shows two peaks, the origin of which is well established. The peaks around 1750 and 1718 meV correspond, respectively, to the neutral exciton of the transition with lowest energy (A exciton) and negative trion (two electrons bound to one hole) [8–10,20]. Both exciton and trion peaks can be fitted by single Lorentzians (solid lines). In contrast, four of the seven investigated flakes show a PL spectrum in which both exciton and trion peaks are split [Fig. 1(d)]. In the following we demonstrate that the splitting of the neutral exciton peak, ranging from 3.5 to 4.7 meV for the flakes investigated (Appendix Sec. 2), can be attributed to Δ_0 as a result of uniaxial strain and intervalley e-h exchange interaction. To this end, we label the peaks at lower and higher energies by the X_X and X_Y excitons, respectively. The observed doublet within the trion emission corresponds to two bright negative trions, intra- and intervalley trions, also arising from the e-h exchange interaction, which recently have been predicted [4,25] and experimentally observed in WS$_2$ [19] and WSe$_2$ [20] monolayers.

II. EXPERIMENTS AND RESULTS

Figure 2(a) shows PL spectra of flake S1 for co- and cross-circularly polarized excitation and detection. In accordance with previous literature, the overall exciton and trion emission lines preserve valley polarization, i.e., the PL intensity for co-polarization (blue curves) is higher than that for cross-polarization (red curves) [8,9]. To distinguish the valley polarizations for X_X and X_Y, we fit the exciton doublet with two Lorentzians (dashed lines) and we define the degree of circular polarization (DCP) as $DCP = (I_{X_{X(Y)}^{K^+}} - I_{X_{X(Y)}^{K^-}})/(I_{X_{X(Y)}^{K^+}} + I_{X_{X(Y)}^{K^-}})$, where $I_{X_{X(Y)}^{K^+}}$ ($I_{X_{X(Y)}^{K^-}}$) is the integrated intensity of the PL for a given circular polarization in detection. We note that the sign of the DCP of the X_X and X_Y peaks is the same and that the DCP value of X_X (29%) is higher than that of X_Y (20%).

Figure 2(b) shows μ-PL spectra of flake S1 with vertically polarized excitation and vertically (green) and horizontally (brown) polarized detection. The overall neutral exciton emission displays a pronounced linear polarization, indicating that the exciton, in addition to the valley polarization [Fig. 2(a)], also preserves valley coherence [8]. In contrast, the trion emission lacks linear polarization, which has been observed before [8] and which has been explained as evidence of the effect
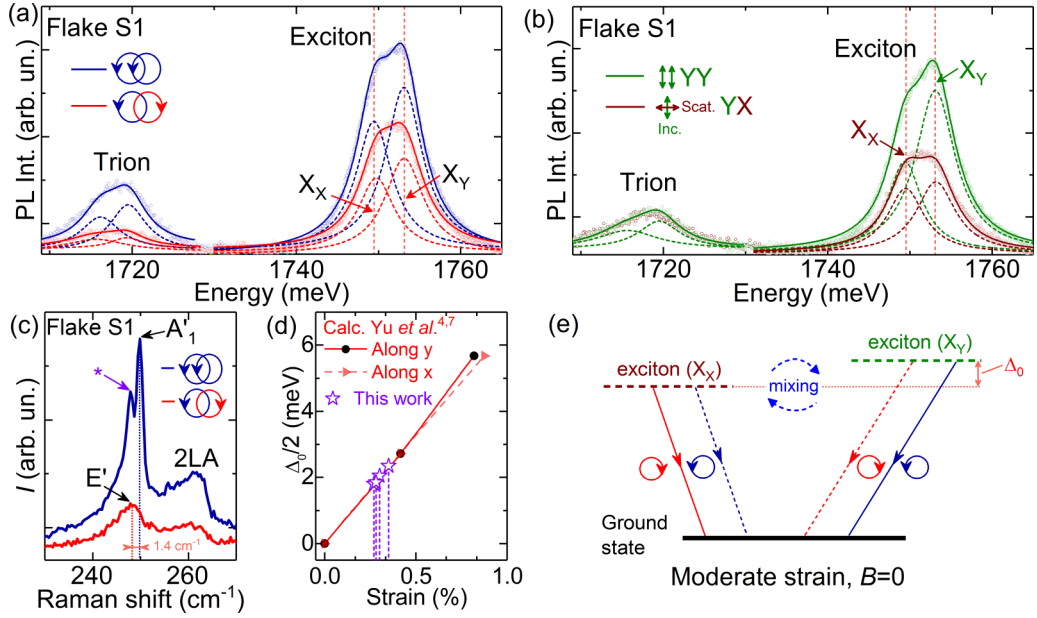
FIG. 2. (a) Circularly polarized PL spectra of flake S1 at 4.2 K for σ^- excitation and σ^- (blue) and σ^+ (red) detection. X_X and X_Y label the vertical and horizontal neutral exciton peaks. Both exciton and trion emission show a pronounced circular polarization (valley polarization). (b) Linearly polarized PL spectra of flake S1 for vertically polarized excitation. Green and brown symbols represent vertically and horizontally polarized detection. The exciton lines are strongly linearly polarized (valley coherence), in contrast to the trion emission (no valley coherence). Dashed lines in (a) and (b) show bi-Lorentzian fits to the doublet structures of the neutral exciton and trion peaks. Solid lines show the total fitted curves. (c) Co- (blue line) and cross- (red line) circularly polarized μ-Raman spectra of WSe_2 flake S1. Dashed lines illustrate the positions of the first-order A_1' and E' modes. An A_1'-E' splitting of 1.4 cm^{-1} demonstrates the presence of a uniaxial strain of about $(0.15 \pm 0.05)\%$. The * symbol indicates a Raman peak that appears only in strained samples. (d) Calculated $\Delta_0/2$ as a function of uniaxial strain, along y (solid line) and x (dashed line) directions based on the model described in Yu et al. [4,25]. Symbols correspond to the Δ_0 values measured by μPL for the four strained ML samples, marked on the calculated line to estimate the amount of strain in the MLs, indicating a strain of $(0.2$–$0.3)\%$. (e) Schematic energy level diagram depicting neutral exciton levels in a strained ML TMD. The combined effect of strain and intervalley e-h exchange results in a mixing of the K^+- and K^--valley excitons. The resulting vertical (X_X) and horizontal (X_Y) exciton peaks, split by Δ_0, are superpositions of K^+ and K^- valley excitons and each emit a combination of σ^+ and σ^- light (or vertically and horizontally polarized light).

of e-h exchange [4,8]. Analogous to the circular polarization case, we fit the exciton doublet (dashed lines) and examine the degree of linear polarization (DLP) of the X_X and X_Y states. $DLP = (I_{X_{X(Y)}^{YY}} - I_{X_{X(Y)}^{YX}})/(I_{X_{X(Y)}^{YY}} + I_{X_{X(Y)}^{YX}})$, where $I_{X_{X(Y)}^{YY}}$ ($I_{X_{X(Y)}^{YX}}$) is the integrated intensity of the PL for the given linear polarization in detection. Remarkably, we find that both X_X and X_Y peaks are linearly polarized with a positive DLP, but that the DLP of X_Y (39%) is three times larger than that of X_X (13%).

Photoluminescence excitation (PLE) measurements (Appendix Sec. 2) show that both excitonic peaks have a finite oscillator strength, which rules out that the low energy peak originates from localized excitons. Instead, polarized μ-Raman spectra [lines in Fig. 2(c), Appendix Sec. 3], measured concomitantly with the μ-PL spectra in Figs. 2(a) and 2(b), demonstrate that the splitting of the neutral exciton emission is caused by uniaxial strain. In σ^-/σ^- polarization the peak at $\sim$249.9 cm^{-1} corresponds to the first-order A_1' phonon mode, whereas the peak at $\sim$248.5 cm^{-1} in σ^-/σ^+ polarization corresponds to the first-order E' phonon mode, in agreement with the Raman selection rules [26–28]. In the absence of strain or in the presence of biaxial strain, i.e., when the in-plane hexagonal structure is preserved, the A_1' and E' Raman modes are degenerate [26,28]. The A_1'-E' splitting,

therefore, indicates the presence of a *uniaxial strain* that breaks the xy-plane symmetry within the ML. An A_1'-E' splitting of 1.4 cm^{-1} corresponds to an estimated uniaxial strain of $\epsilon = 0.15 \pm 0.05\%$ [28]. Further evidence for the presence of uniaxial strain in flake S1 is given by the observation of an additional Raman feature at 247.8 cm^{-1} in the σ^-/σ^- configuration [star-labelled peak in Fig. 2(c)]. This peak is absent for the unstrained flake U1 and is not related to known first- and second-order phonon modes, observed at $\sim$245 cm^{-1}, $\sim$258 cm^{-1}, and $\sim$262 cm^{-1} for both strained and unstrained flakes [27–30]. Instead, the laser wavelength and polarization dependence of this peak suggests that it is associated with a resonant second-order process activated due to the shift of the phonon branches at the M or K points in the presence of uniaxial strain. Finally, the Δ_0 values measured by μ-PL allow an alternative estimation of the strain levels in our ML samples. *Ab initio* calculations permit us to determine the value of the in-plane Zeeman field splitting ($\Delta_0/2$) as a function of the level of uniaxial strain [red curves in Fig. 2(d)] [4]. By matching the Δ_0 values [symbols in Fig. 2(d)] to the calculated lines, we obtain ϵ values of 0.2–0.3%, which agrees well with the results obtained by Raman spectroscopy.

Figure 2(e) summarizes the level structure and optical properties of excitons in strained ML TMDs in a X-Y basis.
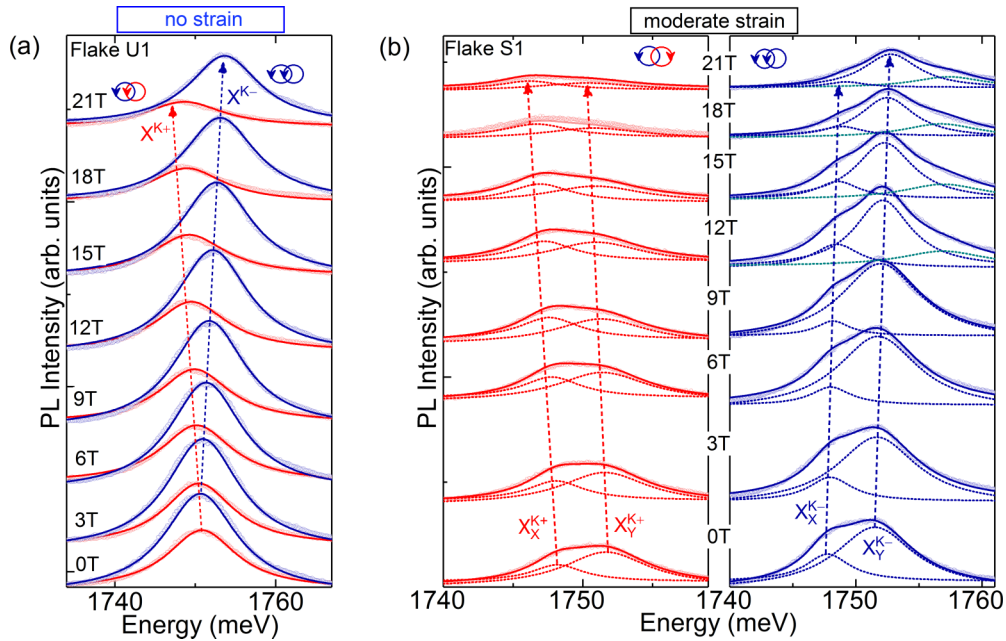
FIG. 3. (a) Low temperature μ-PL spectra (open symbols) of unstrained WSe$_2$ flake U1 at selected magnetic fields. σ^- polarized light was used for excitation, with detection in σ^+ (red) and σ^- (blue) polarization. Solid lines show the Lorentzian fits to the spectra, which are offset vertically for clarity. As a result of the breaking of the time-reversal symmetry the magnetic field lifts the valley degeneracy (valley Zeeman effect). (b) Low temperature μ-PL spectra (open symbols) of strained WSe$_2$ flake S1. σ^- polarized light was used for excitation, with detection in σ^+ (red, left panel) and σ^- (blue, right panel) polarization. Dashed lines denote the bi-Lorentzian fits of the exciton doublet and the solid lines are the total fits of the spectra. In field four excitonic emission lines (X_X^{K+}, X_Y^{K+}, X_X^{K-}, X_Y^{K-}) are visible, associated with vertical (X_Y) and horizontal (X_X) excitons at the K$^+$ and K$^-$ valleys. In high fields an extra PL shoulder emerges in σ^- polarization, such that an extra PL component (green dashed line) is required to fit the total PL spectrum. The red (blue) dashed arrows guide the eye to the linear magnetic shift of the X^{K+} (X^{K-}) peaks towards lower (higher) energy, whereas the green dashed arrow visualizes the appearance of the extra PL line at high fields.

Uniaxial strain breaks rotational symmetry and leads to a finite splitting Δ_0 at $K_{||} = 0$ [Fig. 1(b), right] and a finite oscillator strength of both states with peculiar circular [Fig. 2(a)] and linear [Fig. 2(b)] polarization properties that reflect mixing of the exciton levels. So far, in literature linear polarization of the neutral exciton peak in TMD MLs is associated with exciton valley coherence [8]. Here we argue that a finite exciton DLP can also arise from the xy-plane asymmetry. More information concerning the full polarization dependence of the neutral exciton PL emission is presented in Ref. [31].

Our μ-Raman characterization shows that almost all flakes investigated show a finite splitting between the A$_1'$ and E$'$ modes. This means that all flakes have a certain amount of strain, which varies across a flake and in between flakes. The precise origin of the (uniaxial) strain is unknown, but it is likely created during sample preparation. Mechanical stretching of the ML in a certain direction during exfoliation with tape can lead to uniaxial strain, which is enhanced upon cooling because of the different thermal expansion coefficients of the lattices of the TMD ML and the underlying SiO$_2$ [32]. For "unstrained" samples, such as flake U1, the strain is so low that Δ_0 is smaller than the linewidth of the PL peaks, prohibiting the observation of the exciton doublet. Only for those samples that have a sufficiently large strain and narrow PL emission (flakes S1–S4) the exciton fine structure can be seen. The decrease of the PL linewidth with increasing strain

is a result of the weakening of the exciton-phonon coupling, as recently has been observed in samples with tunable applied uniaxial tensile strain [33]. This provides an additional confirmation of uniaxial strain presence in our WSe$_2$ MLs.

The mixed exciton fine structure of Fig. 2(e) is confirmed by the magnetic response of strained WSe$_2$ MLs [Fig. 3(b) and Appendix Figs. 11 and 12]. The neutral exciton peak of flake U1 splits into two components with increasing field strength, coined as the *valley Zeeman effect* [9–13] (Appendix Sec. 4). Remarkably, in the strained flake S1 both components of the exciton doublet split up in field, resulting in *four* distinct PL lines at high fields [X_X^{K+}, X_Y^{K+}, X_X^{K-}, and X_Y^{K-} in Fig. 3(b)]. As in unstrained samples, the exciton PL associated with the K$^+$ valley (X^{K+}) shifts to low energy, whereas that of the K$^-$ valley (X^{K-}) shifts towards high energy, but each of these peaks now consists of two components. The emergence of four states in an external magnetic field is a result of the splitting of two anisotropic exciton states (along the x or y directions) at zero magnetic field with comparable finite oscillator strengths. This is a consequence of the presence of an in-plane (xy) uniaxial strain. Additional theoretical and computational investigation is needed to better understand the origin of this feature. Moreover, the origin of the spectral feature around 1756 meV [green lines in right panel Fig. 3(b)] is unknown and is probably related to the effect of strain and magnetic field, because it is absent in unstrained flakes.
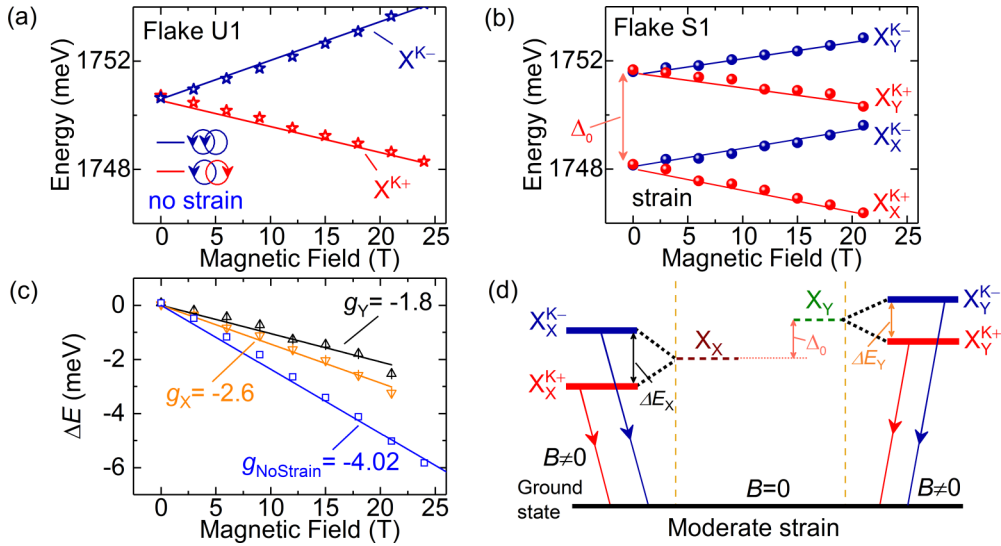
FIG. 4. (a) Transition energies as a function of magnetic field for unstrained WSe_2 flake U1 for σ^+ (red) and σ^- (blue) polarized light. The peak energies shift linearly with field strength (solid lines). (b) Transition energies versus magnetic field for strained WSe_2 flake S1. Both emission lines at 0 T, separated by Δ_0, split up into two and shift linearly with field strength (solid lines). The upper states (X_Y^{K-} and X_X^{K-}) are σ^- polarized (blue) and the lower states (X_Y^{K+} and X_X^{K+}) σ^+ polarized (red). (c) Zeeman splitting ΔE for strained and unstrained ML WSe_2. The lines are linear fits to the data using $\Delta E = g\mu_B B$ resulting to the indicated effective exciton g factors. (d) Schematic of the bright exciton level diagram in a X-Y basis for strained ML TMDs in the presence of an external magnetic field. ΔE_Y and ΔE_X label the magnetic field induced longitudinal and transversal exciton valley splitting.

III. DISCUSSION

All magneto-PL spectra have been fitted by Lorentzian lineshapes (solid and dashed lines Fig. 3), leading to the quantitative analysis of the valley Zeeman effect and the related exciton g factors in Figs. 4(a)–4(c). The energy separation ΔE between σ^+ and σ^- polarized components of each peak increases linearly with field strength B [Fig. 4(c)]. To extract exciton g factors, we define the valley splitting as $\Delta E = g\mu_B B$, where $\mu_B = 0.058$ meV/T is the Bohr magneton [10,13]. This results in a g factor of $g_{NoStrain} \simeq -4.02 \pm 0.05$ for the unstrained flake U1, in agreement with literature values [5,9,11,12]. The splittings of the X_Y and X_X lines are approximately twice smaller than the valley Zeeman splitting, resulting in $g_Y \simeq -1.8 \pm 0.05$ and $g_X \simeq -2.6 \pm 0.05$, indicating that strain reduces significantly the exciton g factor. In TMD MLs, the contribution to the splitting of the PL in magnetic fields comes from two terms: (i) the intrinsic atomiclike orbital momentum of the valence band states, $+2\mu_B$ and $-2\mu_B$ in opposite valleys, this gives an exciton g factor equal to $-4\mu_B$, and (ii) the valley orbital momentum contribution coming from the extended part of the Bloch states (see Appendix Sec. 4) [9–13,34]. This term explains the deviation from $-4\mu_B$ and is related to inequivalent effective masses of electrons (m_e) and holes (m_h) [12]. To account for this effect we fitted the data in Fig. 4(c) with $\Delta E = -\mu_B B(4 + 2\Delta\alpha)$ [10], where $\Delta\alpha = (m_0/m_e - m_0/m_h)$ (m_0 is the electron rest mass) stands for the intercellular contribution to the valley exciton splitting. We find $\Delta\alpha_Y \simeq -0.63$ and $\Delta\alpha_X \simeq -1.18$ for the X_Y and X_X excitons, respectively. These parameters allow us to extract the amount of strain in our sample, following a procedure previously used for ML MoS_2 [13,35]. This leads to $\epsilon \simeq 0.25 \pm 0.05\%$, which agrees well with the values

obtained above by μ-PL and μ-Raman (Fig. 2). Figure 4(d) schematically summarizes the effect of strain in the presence of an external magnetic field in a X-Y exciton basis, in the extension of Fig. 2(e).

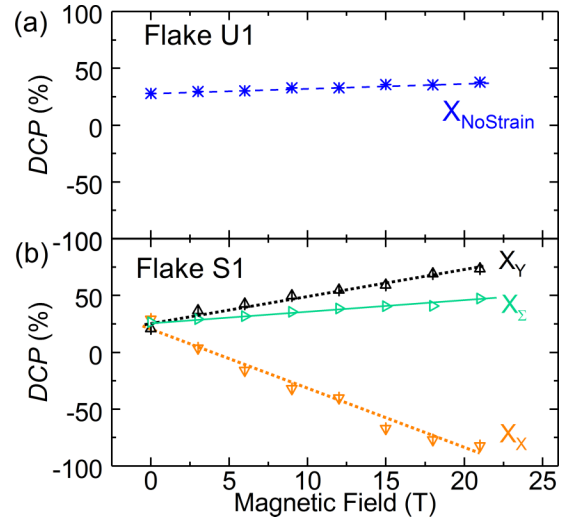Finally, our data resolves apparent discrepancies in literature concerning the magneto-optical properties of WSe_2 MLs,

FIG. 5. Analysis of the valley polarization properties for unstrained (flake U1) and strained (flake S1) WSe_2 MLs. (a) Experimental $DCP(B)$ for WSe_2 ML flake U1. The $DCP(B)$ is roughly constant. (b) Experimental $DCP(B)$ for strained WSe_2 ML flake S1. The $DCP(B)$ of the total PL emission (green symbols) increases with field, whereas the $DCP(B)$ of the X_Y and X_X lines display a more complex behavior.

such as the exciton g factor and the magnetic field induced $DCP(B)$. Aivazian *et al.* [10] reported a spread in measured g factors ($-1.57 \mu_B$ to $-2.86 \mu_B$) and a field-dependent DCP, as opposed to g factors of about $-4 \mu_B$ and constant $DCP(B)$ values reported by others [9,11]. The valley splitting of our unstrained flakes ($g \simeq -4.02 \pm 0.05$ and $g \simeq -4.60 \pm 0.05$ for flakes U1 and U2, respectively) agrees well with the expected splitting of $-4 \mu_B$ [9–11]. Therefore, the electron-hole asymmetry in unstrained samples is small and makes no significant contribution to the observed valley splitting. The small deviation from $-4 \mu_B$ indicates that $\Delta \alpha$ parameter is nonzero but small (-0.02 to $-0.6 \mu_B$). This implies that the carriers in unstrained samples still behave as massive Dirac fermions [1,34]. In addition, unstrained samples show a field-independent $DCP(B)$ (Fig. 5). In contrast, the exciton g factors of *strained* flakes exhibit values around $-2 \mu_B$, a complex field dependence of the PL intensity [Fig. 3(b), Appendix Figs. 11 and 12] and a field-dependent $DCP(B)$ (Fig. 5 and Appendix Sec. 5). As a result, $\Delta \alpha$ is large, demonstrating that strain distorts the band structure, leading to a modification of the massive Dirac fermion model (Appendix Sec. 4).

IV. CONCLUSION

In conclusion, high-resolution magnetophotoluminescence experiments on WSe$_2$ MLs with uniaxial strain reveal the predicted splitting of the neutral exciton emission. Determination of the splitting allows for a direct quantitative comparison between experiment and theory [4] and resolves apparent discrepancies in literature, since crucial parameters of valley excitons, such as their center-of-mass dispersion and g factors, are strain dependent, as well as the inter- and intravalley scattering rates. Our findings are crucially important to understand, design, and realize photonic and optoelectronic devices with valley functionality [2]. To preserve valley polarization and coherence, strain should be strictly avoided, because it leads to mixing of the valleys and relaxation of the valley-selection rules. On the other hand, the controlled use of strain gives the opportunity to vary the excitonic g factor for spintronic applications and the exciton dispersion for polaritonic devices.

APPENDIX: MATERIALS, METHODS, AND ADDITIONAL SUPPORTING INFORMATION

This appendix provides additional data on WSe$_2$ monolayers in the absence and in high magnetic fields.

1. Materials and Methods

In our investigations we have made use of WSe$_2$ monolayer samples mechanically exfoliated and transferred onto SiO$_2$/Si substrates [36]. All microphotoluminescence (μPL), microphotoluminescence excitation (μPLE), and micro-Raman (μ-Raman) measurements were performed using a continuous-wave titanium-sapphire (Ti:Sap) laser at low temperature (4.2 K) and a high-resolution triple-grating spectrometer in subtractive mode. Combining the high-resolution setup with high magnetic fields allows us to probe the fine structure of bright neutral A exciton in monolayer WSe$_2$. For the measurements, the WSe$_2$ monolayer sample was mounted on piezoelectric x-y-z translation stages allowing us to scan over the sample surface with a submicrometer precision. The monolayer sample was excited via a microscope objective with an excitation beam diameter on the sample smaller than 2 μm. With our setup the linear and circular polarization of the excitation and detection can be controlled independently. The optical system was cooled using helium exchange gas and placed inside a liquid helium bath cryostat inserted in a Florida-Bitter magnet generating magnetic fields up to $B = 30$ T. The μPL, μPLE, and μ-Raman spectra were recorded with a multichannel charge-coupled device cooled with liquid nitrogen.

2. Zero field characterization

Data from additional WSe$_2$ monolayers. Figures 6(a) and 6(b) show the unpolarized μ-PL spectra of ML Flakes S1 and S4, exhibiting the typical emission lines for the neutral
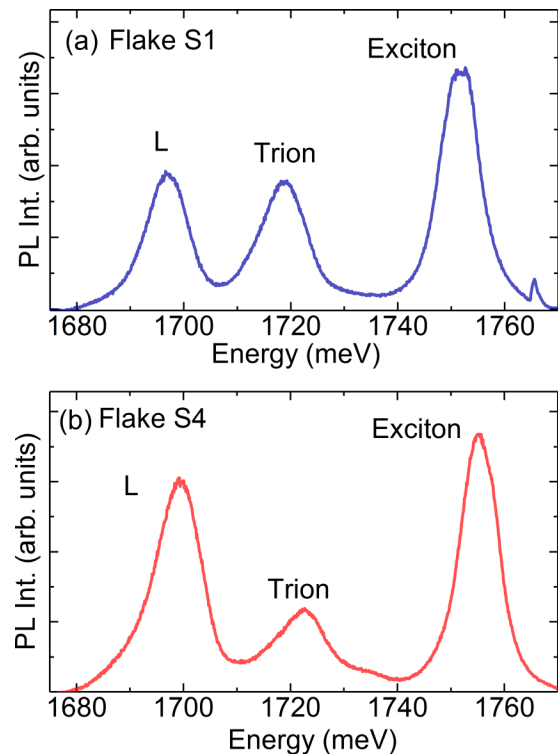

FIG. 6. Photoluminescence characterization using a regular single-grating spectrometer. Unpolarized μ-PL spectra of WSe$_2$ ML flakes S1 (a) and S4 (b) at $T = 4.2$ K.
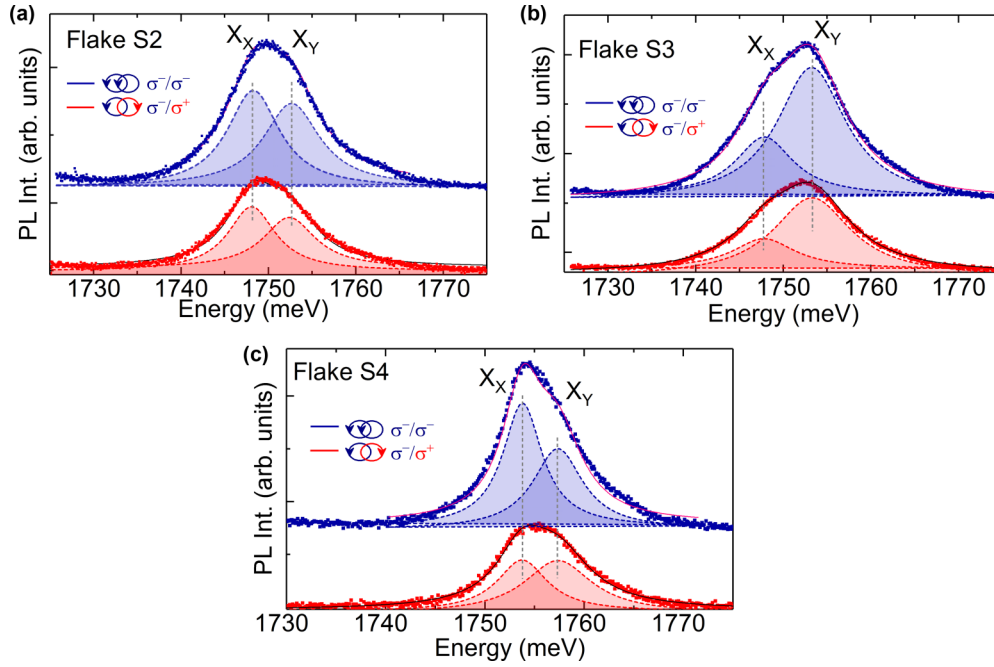
FIG. 7. High resolution polarization-resolved μ-PL spectra of WSe_2 ML flakes S2 (a), S3 (b), and S4 (c). The measured PL spectra are indicated by the symbols, with blue (red) colors for σ^-/σ^- (σ^-/σ^+) excitation/detection polarizations. Lorentzian fits to the X_Y and X_X peaks are given by the dashed lines, where the filled areas show the fitted individual peaks; solid black (pink) lines are the fits to the measured spectra. Δ_0 is the energy splitting between the X and Y exciton branches within the light cone, the position of which are indicated by the vertical dashed gray lines.

exciton around 1750 meV, the negative trion around 1720 meV, and localized excitons around 1695 meV [8,9,37,38]. From the exciton/trion intensity ratio we estimate the background carrier density n in our samples to be around 0.4×10^{12} cm^{-2} at low excitation power (10 μW). The exciton/trion intensity ratio is fairly constant across all samples [Figs. 1(c) and 1(d) of the main text and Figs. 6(a) and 6(b)], which means that the doping levels of the samples do not vary significantly, despite the fact that the samples have been exfoliated from different WSe_2 bulk crystals.

Figure 7 shows high resolution, circular polarization-resolved μ-PL spectra of ML flakes S2, S3, and S4. These samples exhibit a doublet peak in the neutral exciton emission, which is attributed to X_Y and X_X excitons. The energy separation Δ_0 between the X_X and X_Y peaks varies from sample to sample, from 3.6 to 4.7 meV. Using σ^-/σ^- and σ^-/σ^+ excitation/detection polarizations, both X_Y and X_X are circularly polarized with a slightly larger circular polarization degree for the X_X peak. All extracted parameters for the strained WSe_2 ML flakes are summarized in Table I.

TABLE I. Extracted parameters for strained WSe_2 monolayer samples.

Flake	Δ_0 (meV)	ϵ (%)	DCP X_Y (%)	DCP X_X (%)
S1	3.7 ± 0.1	0.26 ± 0.05	20	29
S2	4.4 ± 0.1	0.30 ± 0.05	24	26
S3	4.7 ± 0.1	0.31 ± 0.05	25	28
S4	3.6 ± 0.1	0.28 ± 0.05	21	42

PLE measurements. Evidence for the exciton fine structure has been given by PLE experiments in different systems such as quasi-2D quantum wells (QWs) and colloidal quantum dots (QDs) [39,40], in which the PL is measured under resonant excitation. A strong absorption occurs predominately when the laser excitation energy is resonant with an excitonic level which has a strong oscillator strength. This can be observed by monitoring the trion (charged exciton) PL emission intensity while varying the excitation energy across the exciton resonance [41].

The PL spectrum of unstrained WSe_2 ML flake U1 shows two peaks, corresponding to the neutral exciton and negative trion of the transition with lowest energy (A exciton) [8–10,20]. In contrast, the strained flake S1 shows a PL spectrum in which both exciton and trion peaks have a fine structure: For the neutral exciton case we label the peaks at lower and higher energies by X_X and X_Y excitons. In Fig. 8, we show the same PL spectra of Figs. 1(c) and 1(d) together with the spectrally-integrated PL intensity of the trion emission [photoluminescence excitation (PLE) experiments, red and orange symbols]. The maximum trion intensity of flake U1 occurs when the excitation laser energy coincides with the exciton emission peak (vertical dashed line). The PLE experiments of flake S1 show that both X_X and X_Y have finite oscillator strength. The absence of a Stokes shift between the maxima in PL and PLE exclude any effects of localization on the exciton emission, which might arise because of defects or disorder in our (strained) WSe_2 MLs, in contrast to what was reported in Ref. [42]. Moreover, our PLE measurements provide further evidence for the energy level diagram presented in Fig. 2(e) of the main text, in which
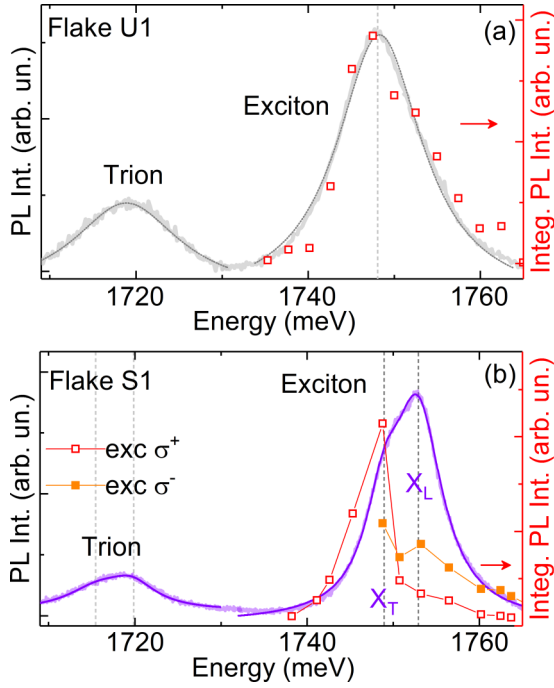
FIG. 8. Unpolarized PL and excitation polarization-resolved PLE spectra of flakes U1 (a) and S1 (b). The PLE spectra are indicated by the symbols. The signal was detected on the trion line in σ^+/σ^+ circular polarization for flake U1 and in σ^+/σ^+ (σ^-/σ^-) excitation/detection polarizations flake S1. The position of the different exciton lines are indicated by the vertical dashed lines.

the combined effect of strain and intervalley e-h exchange results in a mixing of the K^+- and K^--valley excitons. The polarization state of X_Y and X_X is described in Sec. S5 by examining the splitting of each exciton branch.
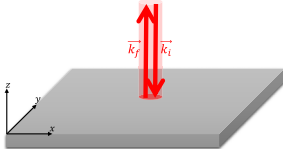
3. Phonon modes and Raman selection rules in ML WSe$_2$

The space group of ML WSe$_2$ is $P\bar{6}m2$ (n° 187 with point group D$_{3h}$). The unit cell of a WSe$_2$ monolayer is composed of three atoms giving rise to nine phonon modes at the Γ point [27]. These phonons are decomposed as $\Gamma = 2A_2'' + A_1' + 2E' + E''$, where the E$'$ and E$''$ modes are each doubly degenerate, leading to modes E$'$(1), E$'$(2), E$''$(1), and E$''$(2), where the indices (1) and (2) differentiate their irreducible matrices.

In the configuration $\bar{z}(\sigma^-, \sigma^-)z$ it is possible to probe the A$_1'$ symmetry but not E$'$. E$'$ phonons can be probed in the configuration $\bar{z}(\sigma^-, \sigma^+)z$ for which $I^{E'(1)} \neq 0$. All Raman selection rules for monolayer WSe$_2$ for linear and circular polarizations in backscattering geometry are summarized in Table II.

According to these Raman selection rules, only the A$_1'$ and E$'$ symmetries are detectable in the configuration we use, i.e., with the incident and scattered light propagating in the z direction with polarization in the xy plane of the flakes. We expect to observe one A$_1'$ and/or one E$'$ optical mode in our spectra (the second E$'$ mode being an acoustic mode) [26–28].

TABLE II. Raman selection rules of monolayer WSe$_2$ for our measurement configuration (shown on top). Porto's notation is used to describe the configuration as $\mathbf{k}_i(\mathbf{e}_i, \mathbf{e}_s)\mathbf{k}_s$. $\mathbf{k}_i$ and $\mathbf{k}_s$ denote the wavevectors of the incident and scattered light. X and Y denote linear polarization along the in-plane x and y directions, σ^+ and σ^- denote respectively right and left circular polarizations.

Configurations	A_1'	$E'(1)$	$E'(2)$	$E''(1)$	$E''(2)$
$\bar{z}(Y, Y)z$	✓	✓	0	0	0
$\bar{z}(Y, X)z$	0	0	✓	0	0
$\bar{z}(X, Y)z$	0	0	✓	0	0
$\bar{z}(X, X)z$	✓	✓	0	0	0
$\bar{z}(\sigma^-, \sigma^-)z$	✓	0	0	0	0
$\bar{z}(\sigma^-, \sigma^+)z$	0	✓	✓	0	0

4. Magnetic field measurements—Data from additional WSe$_2$ monolayers

The *valley Zeeman effect* is a phenomenon recently observed in monolayer transition-metal dichalcogenides [9–12,43,44]. It originates from the different magnetic
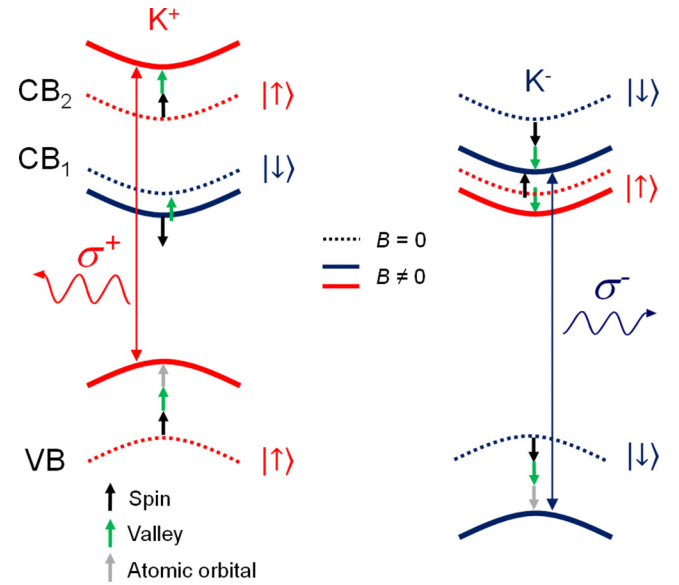

FIG. 9. Evolution of the conduction and valence bands in a WSe$_2$ ML with applied magnetic field. Dashed lines indicate the energetic position of the spin-split conduction (CB$_1$ and CB$_2$) and valence (VB) bands in a WSe$_2$ ML at zero magnetic field. Solid lines denote the energy levels in an applied magnetic field. Small red (blue) arrows indicate spin up (down). The field-induced changes are caused by the spin, valley, and atomical orbital magnetic moments, indicated by, respectively, small black, green, and gray arrows. Optical transitions (solid vertical arrows) preserve spin and lead to σ^+- and σ^--polarized light. The transition to the CB$_1$ level is optically inactive in W-based MLs and is, therefore, omitted in this work.

TABLE III. Contributions to the magnetic moments in the conduction (CB$_2$) and valence (VB) bands in WSe$_2$ monolayers.

Magnetic moments	CB$_2$ (K$^+$)	VB (K$^+$)	CB$_2$ (K$^-$)	VB (K$^-$)
Spin	$+\mu_B$	$+\mu_B$	$-\mu_B$	$-\mu_B$
Atomic orbital	0	$+2\mu_B$	0	$-2\mu_B$
Valley	$+\alpha\mu_B$	$+\alpha\mu_B$	$-\alpha\mu_B$	$+\alpha\mu_B$

moments in the K$^+$ and K$^-$ valleys. For clarification, we depict in Fig. 9 the evolution of the conduction (CB) and valence (VB) bands in WSe$_2$ or WS$_2$ MLs with an applied out-of-plane magnetic field (Faraday geometry). In this approximation we only take into account the uppermost VB and we neglect the lower spin-split VB. The red (blue) colors indicate the spin-up (down) levels.

In zero external magnetic field, the K$^+$ and K$^-$ valleys are degenerate because of time-reversal symmetry. In field, the valley degeneracy is lifted, which comes from the sum of three contributions to the magnetic moments of both the CB (μ^c) and VB (μ^b): the spin (μ_S), atomiclike orbital (μ_a), and valley (μ_v) magnetic moments. The overall splitting of the PL spectra in magnetic fields is given by: $\Delta E = \Delta E^c - \Delta E^v = (\mu^c - \mu^b)B$.

First of all, spin does not contribute to the observed valley Zeeman effect, because the optical transitions conserve the spin. For allowed transitions the CB and VB shift in the same direction so that the spin magnetic moment μ_S can be ignored (black arrows in Fig. 9).

The main contribution to the field-induced splitting comes from the intrinsic atomiclike orbital momentum μ_a. In the literature this component is generally referred to as the *intracellular* component. The origin of this component is related to the character of the bands around the K points of the Brillouin zone: The energy levels in the conduction band originate from the hybridization of the d and p orbitals of W and Se atoms, which provides the carriers with an in-plane angular momentum $l_z = 0$. The valence band is composed of the d orbitals of the W atoms with $l_z = \pm 2$. The contribution to the magnetic moment from the atomic orbitals is then $\mu_a = l_z \mu_B$. Since there is no contribution from the conduction band ($\mu_a^c = 0$), the total contribution from the atomic magnetic moment is $\mu_a^c - \mu_a^v = \pm 2 \mu_B$.

The last component that contributes to the splitting observed in magnetic field measurements is the valley magnetic moment and originates from the phase winding of the Bloch functions referred to as the *intercellular* component [34]. In each of the valleys, the valley magnetic moments are equal in magnitude but have opposite sign $\mu^{K+} = -\mu^{K+}$ and can be estimated by $\mu_v = \alpha_{c,v} \tau \mu_B$, where $\tau = \pm 1$ represents the valley index [$\tau = +1$ (-1) for K$^+$ (K$^-$)] and $\alpha_c = m_0/m_e$ for the conduction band and $\alpha_v = m_0/m_h$ for the valence band. This implies that when $m_e = m_h$ there is no net contribution from the valley magnetic moment. However, if $m_e \neq m_h$, there will be a finite contribution in the K$^\pm$ valley equal to $\pm(m_0/m_e - m_0/m_h)\mu_B$.

All magnetic moments for both conduction and valence bands in monolayer WSe$_2$ are summarized in Table III. The
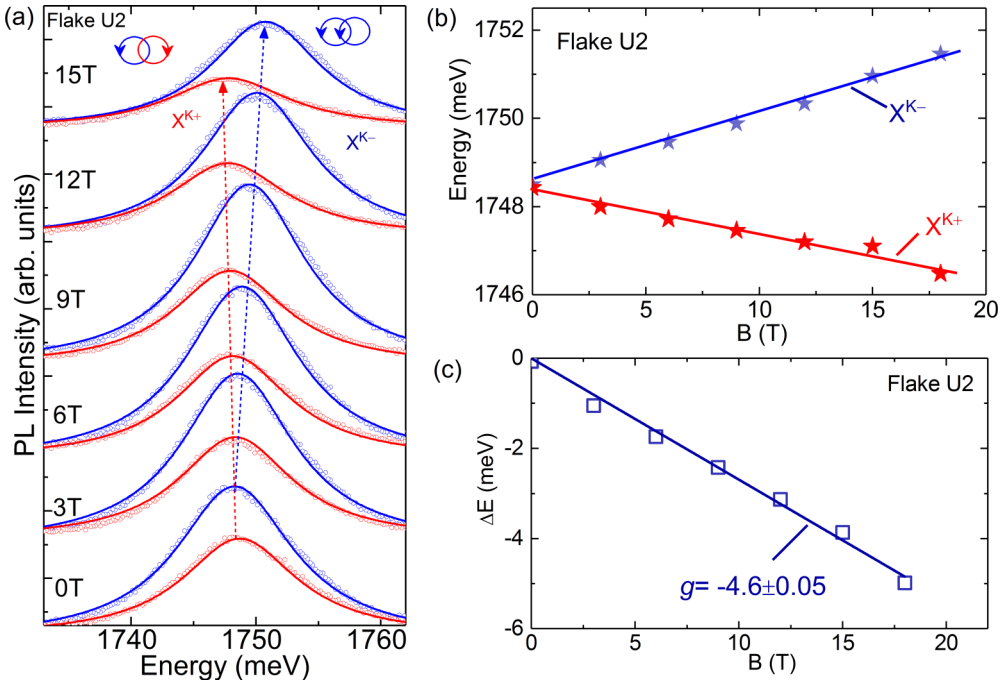

FIG. 10. PL emission of WSe$_2$ ML flake U2 in an external magnetic field (Faraday geometry). (a) Low temperature (4.2 K) μ-PL spectra of flake U2 at selected magnetic fields. σ^- polarized light was used for excitation, with detection in σ^+ (red) and σ^- (blue) polarization. Solid lines show the Lorentzian fits to the spectra. The red (blue) dashed arrows guide the eye to the linear magnetic shift of the X^{K+} and X^{K-} peaks towards lower (higher) energy. Spectra and fits are shifted vertically for clarity. (b) Corresponding transition energies as a function of magnetic field for σ^+ (red) and σ^- (blue) polarized detection. The peak energies shift linearly with field strength (solid lines). (c) Zeeman splitting ΔE of flake U2 for the neutral exciton peaks. The solid line is a linear fit to the data using $\Delta E = g\mu_B B$ resulting in the indicated effective exciton g factor.
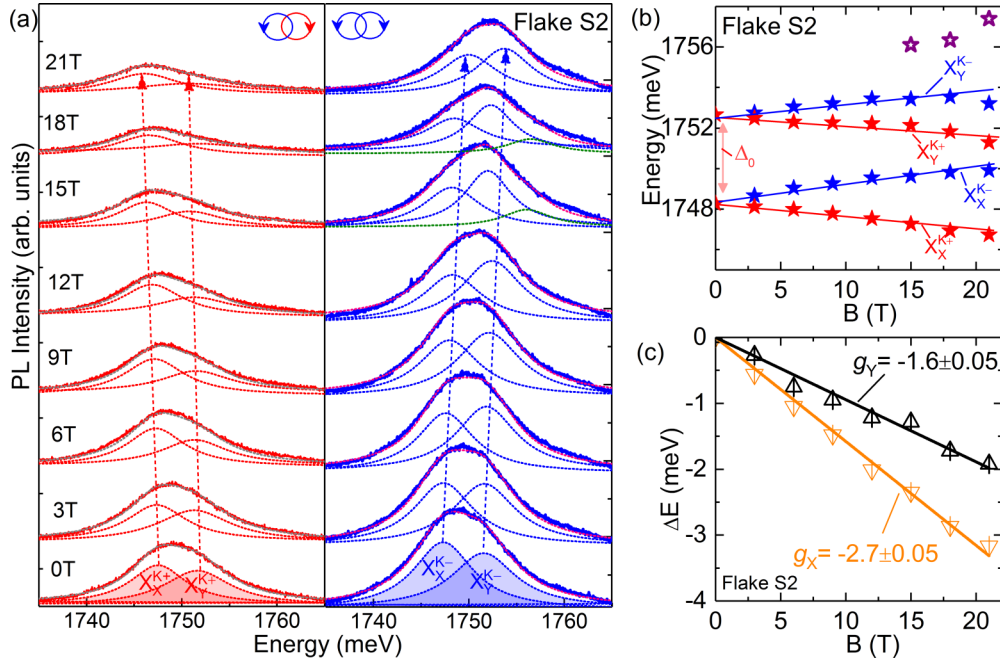
FIG. 11. PL emission of WSe$_2$ ML flake S2 in an external magnetic field (Faraday geometry). (a) Low temperature (4.2 K) μ-PL spectra of flake S2 at selected magnetic fields. σ^- polarized light was used for excitation, with detection in σ^+ (red, left panel) and σ^- (blue, right panel) polarization. Solid lines show the Lorentzian fits to the spectra, obtained by fitting double-Lorentzian peaks (dashed lines). The red (blue) dashed arrows guide the eye to the linear magnetic shift of the X_X^{K+} and X_Y^{K+} (X_X^{K-} and X_Y^{K-}) peaks towards lower (higher) energy. Spectra and fits are shifted vertically for clarity. (b) Corresponding transition energies as a function of magnetic field for σ^+ (red) and σ^- (blue) polarized detection. The peak energies shift linearly with field strength (solid lines). (c) Zeeman splitting ΔE of flake S2 for the X_X and X_Y peaks. The solid lines are linear fits to the data using $\Delta E = g\mu_B B$ resulting in the indicated effective exciton g factors.

valley Zeeman splitting observed in the PL is $\Delta E = (\mu_s + \mu_a + \mu_v)B \simeq -4\mu_B B$. This corresponds to an expected splitting of the PL lines of $\simeq 8$ meV at the maximum field of 30 T, which is similar to what we observe in all experiments for the neutral exciton.

Figure 10(a) shows the PL spectra of an *unstrained* WSe$_2$ ML (flake U2) in the presence of an external magnetic field, taken with σ^- polarized laser excitation and with σ^+ and σ^- detection polarization. The exciton PL has been fitted using one Lorentzian function to extract the integrated intensity and the peak energy as a function of magnetic field. The results of this analysis are shown in Figs. 10(b) and 10(c). The behavior of this flake is similar to that of flake U1 [Figs. 3(a), 4(a) and 4(c) in the main text]. The valley Zeeman splitting [Fig. 10(c)] increases linearly with field and can be described with a g factor of -4.60 ± 0.05 μ_B. Thus, the contribution from the valley magnetic moment in unstrained TMD monolayers is finite but small ($\simeq \pm 0.6$ μ_B).

A similar analysis has been performed on the *strained* MLs (flakes S1, S2, and S3). For these samples the transition energies are obtained by fitting the exciton peaks to double Lorentzians for both cross- and co-polarization. Figure 11 shows the experimental data for the strained flake S2. The effective g factors for the X_Y and X_X exciton peaks are determined from Fig. 11(c), resulting in $g_Y \simeq -1.6 \pm 0.05$ for X_Y and $g_X \simeq -2.7 \pm 0.05$ for X_X. The absolute values of both exciton g factors are significantly lower than 4, analogous to the results of flake S1 [Figs. 3(b), 4(b) and 4(c) of the main text] and S3.

Note that for one out of four strained WSe$_2$ monolayer flakes (flake S4), we obtained larger g-factor values ($g_Y \simeq -3.5$ μ_B and $g_X \simeq -3.8$ μ_B) (see Fig. 12). We explain this finding by the presence of strain in the sample that preserves the in-plane symmetry of the ML, which is supported by the Raman spectra of that sample (Fig. 13) which shows degenerate $[A_1'(\Gamma)]$ and $[E'(\Gamma)]$ modes.

It has been shown by Xiao *et al.* [34] that the carriers in a direct-gap monolayer TMD in the vicinity of the $K^\pm$ points can be described by a simple tight-binding Hamiltonian:

$$\hat{H} = \hbar v_F(\tau q_x \sigma_x + q_y \sigma_y) + \Delta\sigma_z,$$

where v_F is the Fermi velocity (which replaces the speed of light and which is constant, independent of the carrier density), τ labels the K^+ and K^- valley, and Δ corresponds to half of the band gap (also so-called "mass gap"); σ_x, σ_y and σ_z are the Pauli matrices defined in a basis consisting of the two d orbitals of the W atoms. The carriers described by this Hamiltonian behave as massive Dirac fermions with a moderate spin-orbit coupling [1,34].

In MLs that are strained along a high-symmetry axis, i.e., uniform uniaxial strain, the low energy Hamiltonian reads [45]:

$$\hat{H}_{\text{strain}} \simeq \hbar v_{F_x} k_x \sigma_x + \tau \hbar v_{F_y} k_y \sigma_y + \Delta\sigma_z$$
$$+ \tau\beta(a_{xx} - a_{yy})\hbar v_F k_y,$$

in which the last term represents a valley-dependent parameter that does not couple to the sublattice pseudospin Pauli
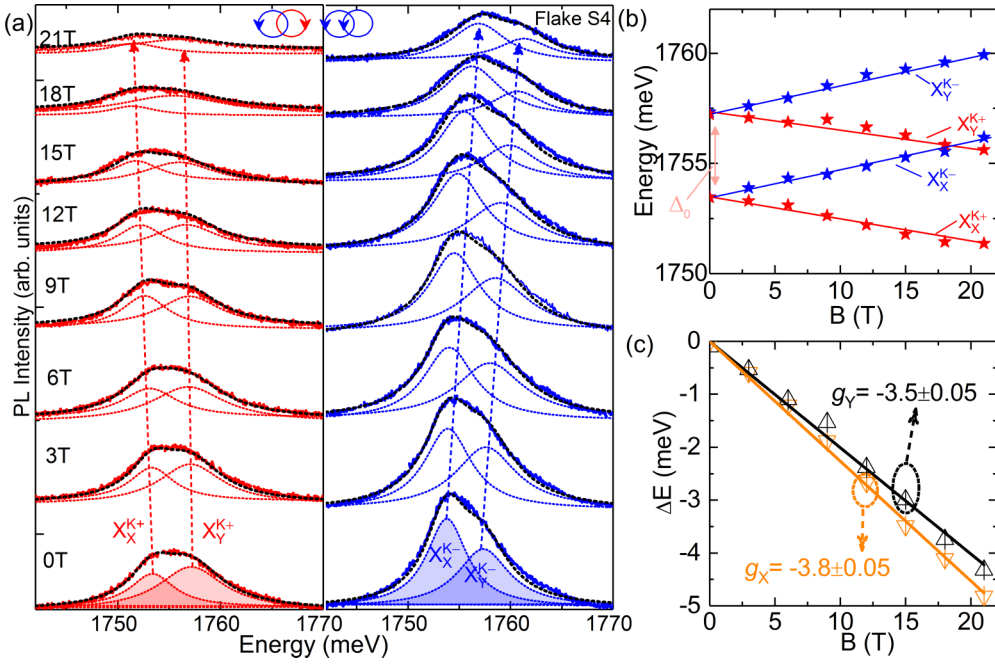
FIG. 12. PL emission of WSe$_2$ ML flake S4 in an external magnetic field (Faraday geometry). (a) Low temperature (4.2 K) μ-PL spectra of flake S4 at selected magnetic fields. σ^- polarized light was used for excitation, with detection in σ^+ (red, left panel) and σ^- (blue, right panel) polarization. Solid lines show the Lorentzian fits to the spectra, obtained by fitting double-Lorentzian peaks (dashed lines). The red (blue) dashed arrows guide the eye to the linear magnetic shift of the X_X^{K+} and X_Y^{K+} (X_X^{K-} and X_Y^{K-}) peaks towards lower (higher) energy. Spectra and fits are shifted vertically for clarity. (b) Corresponding transition energies as a function of magnetic field for σ^+ (red) and σ^- (blue) polarized detection. The peak energies shift linearly with field strength (solid lines). (c) Zeeman splitting Δ_0 of flake S4 for the X_X and X_Y peaks.

matrices. β is a dimensionless parameter on the order of unity and a_{ij} are the components of the strain tensor [45]. The
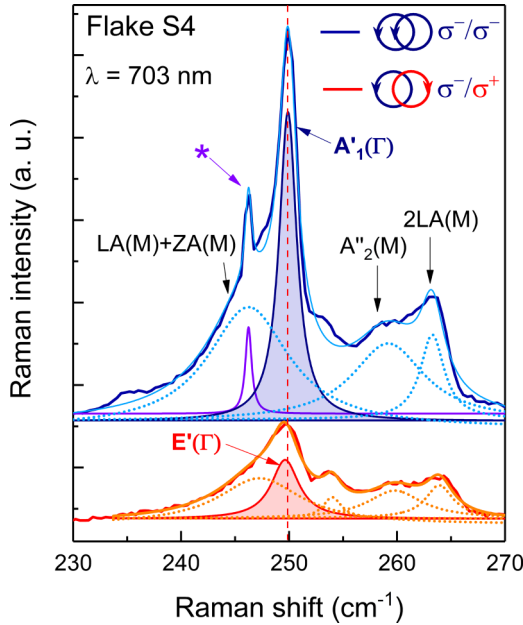

FIG. 13. Raman characterization of flake S4. Low temperature (4.2 K) μ-Raman spectra of WSe$_2$ monolayer sample S4, with co- and cross circularly polarized excitation and detection. Excitation wavelength was 703 nm. Flake S4 is strained because it exhibits a splitting in the neutral exciton peak (see Fig. 12), but no shift was observed between the $[A_1'(\Gamma)]$ and $[E'(\Gamma)]$ modes, indicating that the in-plane hexagonal symmetry is preserved.

main effects of the uniaxial strain are the change in the Fermi velocity υ_F because of the broken rotational symmetry and the modification of the energy gap Δ which directly affects the exciton properties.

The $\Delta\alpha$ parameter extracted from our magneto-PL measurements allows us to determine how much the behavior of the carriers deviates from the massive Dirac fermion model. In unstrained samples, the PL exhibits a single exciton peak, $\Delta\alpha \simeq 0$ and thus $g \simeq -4.0 \pm 0.5$, and the carriers behave as massive Dirac carriers described by $\hat{H}$. However, in strained samples, $\Delta\alpha$ is large and the absolute value of the g factor $|g| < 4.0$. Because the band structure is distorted and roughly can be characterized by the strained Hamiltonian $\hat{H}_{strain}$, the carriers in a strained sample deviate from the massive Dirac fermions model.

5. Degree of circular polarization in magnetic fields

In this section we examine the magnetic field dependence of the exciton degree of circular polarization $[DCP(B)]$ for (un)strained WSe$_2$ MLs [Fig. 14(a)]. The $DCP(B)$ is defined as $DCP(B) = (I_{X^{K+}} - I_{X^{K-}})/(I_{X^{K+}} + I_{X^{K-}})$, where $I_{X^{K+}}$ ($I_{X^{K-}}$) is the integrated intensity of the PL for σ^+ (σ^-) polarization in detection. Figure 14 shows the results of the analysis of the field dependent PL of flakes U1 and S1 (corresponding to the results in Fig. 3 of the main text). The $DCP(B)$ of the unstrained flake U1 [blue symbols in Fig. 14(a)] is roughly constant with field ($\simeq 25\%$), in agreement with most reports in literature [11,12]. The valley polarization of about 25% is governed by the selective excitation in one valley and exciton relaxation that partly conserves valley
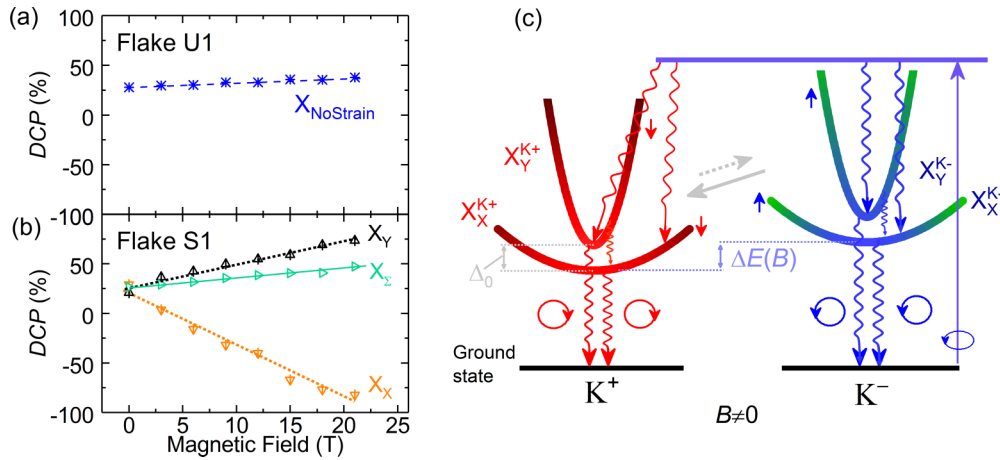
FIG. 14. Analysis of the valley polarization properties for unstrained (flake U1) and strained (flake S1) WSe$_2$ MLs. (a) Experimental $DCP(B)$ for WSe$_2$ ML flake U1. The $DCP(B)$ is roughly constant. (b) Experimental $DCP(B)$ for strained WSe$_2$ ML flake S1. The $DCP(B)$ of the total PL emission (green symbols) increases with field, whereas the $DCP(B)$ of the X$_Y$ and X$_X$ lines display a more complex behavior. (c) Valley-based picture of the bright exciton energy level structure, to describe the evolution of the DCP in magnetic field. The solid arrow depicts optical excitation in σ^- polarization. Wavy arrows denote intra- and intervalley scattering events.

index (pseudospin). Upon σ^- excitation the σ^--polarized PL emission remains dominant at all field strengths [Fig. 3(a), main text], which shows that repopulation across the Zeeman split valley-exciton levels is not important, even if the X^{K+} level is lowest in energy at high fields. The $DCP(B)$ of the strained flake S1 [green symbols in 14(b)] shows different behavior. The valley polarization of about 25% at zero field increases to 50% at 20 T. This behavior resembles the one reported for WSe$_2$ by Aivazian *et al.* [10], who attributed this characteristic X pattern to a distinct exciton dispersion. Here we relate this DCP pattern to the effect of strain on the exciton fine structure, where the DCP of unstrained MLs is constant with field [11,12].

The strain in the sample is accompanied by a splitting of the exciton peak in four peaks in high fields [Fig. 14(c)] and with a reduction in the exciton g factors. The precise field dependence of all four peaks appears to be very complex [Fig. 3(b), main text]. At low magnetic fields, X$_Y$ is slightly

more intense than X$_X$ in both circular polarizations. In co-polarization X$_Y$ becomes really dominant at the highest fields, whereas in cross-polarization X$_X$ becomes brighter than X$_Y$. This complex behavior is further illustrated by distinguishing between the g factors of the X$_Y$ and X$_X$ transitions. The $DCP(B)$ of X$_Y$ [black symbols in Fig. 14(b)] increases monotonically from 20% at 0 T to 73% at 21 T. The DCP for X$_X$ (orange symbols, 29% at 0 T) gradually decreases and, eventually, changes sign to become negative (-82%). These remarkable results should be analyzed considering the intra- and intervalley scattering processes within a valley-based exciton picture [Fig. 14(c)]. The decrease in DCP for X$_X$ occurs because at high fields the X_X^{K+} state becomes the lowest state and is readily populated because strain and e-h exchange mixes all exciton levels. The precise nature of the opposite trend of the DCP with field for X$_X$ and X$_Y$ requires further investigation, but this data clearly reflects the distinctive nature of the X$_X$ and X$_Y$ exciton branches.

[1] X. Xu, W. Yao, D. Xiao, and T. F. Heinz, Spin and pseudospins in layered transition metal dichalcogenides, Nat. Phys. **10**, 343 (2014).

[2] K. F. Mak and J. Shan, Photonics and optoelectronics of 2D semiconductor transition metal dichalcogenides, Nat. Photon. **10**, 216 (2016).

[3] J. R. Schaibley, H. Yu, G. Clark, P. Rivera, J. S. Ross, K. L. Seyler, W. Yao, and X. Xu, Valleytronics in 2D materials, Nat. Rev. Mater. **1**, 16055 (2016).

[4] H. Yu, X. Cui, X. Xu, and W. Yao, Valley excitons in two-dimensional semiconductors, Nat. Sci. Rev. **2**, 57 (2015).

[5] M. Koperski, M. R Molas, A. Arora, K. Nogajewski, A. O. Slobodeniuk, C. Faugeras, and M. Potemski, Optical properties of atomically thin transition metal dichalcogenides: Observations and puzzles, Nanophotonics **6**, 1289 (2017).

[6] K. F. Mak, K. He, C. Lee, G. H. Lee, J. Honeand, T. F. Heinz, and J. Shan, Tightly bound trions in monolayer MoS$_2$, Nat. Mater. **12**, 207 (2013).

[7] T. Cao, G. Wang, W. Han, H. Ye, C. Zhu, J. Shi, Q. Niu, P. Tan, E. W. Baoli Liu, and J. Feng, Valley-selective circular dichroism of monolayer molybdenum disulphide, Nat. Commun. **3**, 887 (2012).

[8] A. M. Jones, H. Yu, N. J. Ghimire, S. Wu, G. Aivazian, J. S. Ross, B. Zhao, J. Yan, D. G. Mandrus, D. Xiao, W. Yao, and X. Xu, Optical generation of excitonic valley coherence in monolayer WSe$_2$, Nat. Nanotech. **8**, 634 (2013).

[9] A. Srivastava, M. Sidler, A. V. Allain, D. S. Lembke, A. Kis, and A. Imamoglu, Valley zeeman effect in elementary optical excitations of a monolayer WSe$_2$, Nat. Phys. **11**, 141 (2015).

[10] G. Aivazian, Z. Gong, A. M Jones, R.-L. Chu, J, Yan, D. G Mandrus, C. Zhang, D. Cobden, W. Yao, and X. Xu, Magnetic

control of valley pseudospin in monolayer WSe$_2$, Nat. Phys. **11**, 148 (2015).

[11] A. A. Mitioglu, P. Plochocka, A. Granados del Aguila, P. C. M. Christianen, G. Deligeorgis, S. Anghel, L. Kulyuk, and D. K. Maude, Optical investigation of monolayer and bulk tungsten diselenide (WSe$_2$) in high magnetic fields, Nano Lett. **15**, 4387 (2015).

[12] G Wang, L Bouet, M M Glazov, T Amand, E L Ivchenko, E Palleau, X Marie, and B Urbaszek, Magneto-optics in transition metal diselenide monolayers, 2D Materials **2**, 034002 (2015).

[13] A. A. Mitioglu, K. Galkowski, A. Surrente, L. Klopotowski, D. Dumcenco, A. Kis, D. K. Maude, and P. Plochocka, Magnetoexcitons in large area CVD-grown monolayer MoS$_2$ and MoSe$_2$ on sapphire, Phys. Rev. B **93**, 165412 (2016).

[14] L. C. Andreani and F. Bassani, Exchange interaction and polariton effects in quantum-well excitons, Phys. Rev. B **41**, 7536 (1990).

[15] M. Z. Maialle, E. A. de Andrada e Silva, and L. J. Sham, Exciton spin dynamics in quantum wells, Phys. Rev. B **47**, 15776 (1993).

[16] M. Bayer, G. Ortner, O. Stern, A. Kuther, A. A. Gorbunov, A. Forchel, P. Hawrylak, S. Fafard, K. Hinzer, T. L. Reinecke, S. N. Walck, J. P. Reithmaier, F. Klopf, and F. Schäfer, Fine structure of neutral and charged excitons in self-assembled In(Ga)As/(Al)GaAs quantum dots, Phys. Rev. B **65**, 195315 (2002).

[17] S. Brovelli, R.-D. Schaller, S.-A. Crooker, F. García-Santamaría, Y. Chen, R. Viswanatha, J. Hollingsworth, H. Htoon, and V.-I. Klimov, Nano-engineered electron-hole exchange interaction controls exciton dynamics in core–shell semiconductor nanocrystals, Nat. Commun. **2**, 280 (2011).

[18] M. M. Glazov, T. Amand, X. Marie, D. Lagarde, L. Bouet, and B. Urbaszek, Exciton fine structure and spin decoherence in monolayers of transition metal dichalcogenides, Phys. Rev. B **89**, 201302 (2014).

[19] G. Plechinger, P. Nagler, A. Arora, R. Schmidt, A. Chernikov, A. Granados del Aguila, P. Christianen, R. Bratschitsch, C. Schuller, and T. Korn, Trion fine structure and coupled spin–valley dynamics in monolayer tungsten disulfide, Nat. Commun. **7**, 12715 (2016).

[20] A. M. Jones, H. Yu, J. R. Schaibley, J. Yan, D. G. Mandrus, T. Taniguchi, K. Watanabe, H. Dery, Yao, and X. Xu, Excitonic luminescence upconversion in a two-dimensional semiconductor, Nat. Phys. **12**, 323 (2016).

[21] M. M. Glazov, E. L. Ivchenko, G. Wang, T. Amand, X. Marie, B. Urbaszek, and B. L. Liu, Spin and valley dynamics of excitons in transition metal dichalcogenide monolayers, Phys. Status Solidi B **252**, 2349 (2015).

[22] S. Donati, L. Dominici, G. Dagvadorj, D. Ballarini, M. De Giorgi, A. Bramati, G. Gigli, Y. G. Rubo, M. H. Szymańska, and D. Sanvitto, Twist of generalized skyrmions and spin vortices in a polariton superfluid, Proc. Natl. Acad. Sci. U.S.A. **113**, 14926 (2016).

[23] R. Balili, B. Nelsen, D. W. Snoke, R. H. Reid, L. Pfeiffer, and K. West, Huge splitting of polariton states in microcavities under stress, Phys. Rev. B **81**, 125311 (2010).

[24] Ł. Kłopotowski, M. D. Martín, A. Amo, L. Viña, I. A. Shelykh, M. M. Glazov, G. Malpuech, A. V. Kavokin, and R. André, Optical anisotropy and pinning of the linear polarization of light

[25] in semiconductor microcavities, Solid State Commun. **139**, 511 (2006).

[25] H. Yu, G.-B. Liu, P. Gong, X. Xu, and W. Yao, Dirac cones and dirac saddle points of bright excitons in monolayer transition metal dichalcogenides, Nat. Commun. **5**, 3876 (2014).

[26] S.-Y. Chen, C. Zheng, M. S. Fuhrer, and J. Yan, Helicity-resolved Raman scattering of MoS$_2$, MoSe$_2$, WS$_2$, and WSe$_2$ atomic layers, Nano Lett. **15**, 2526 (2015).

[27] X. Zhang, X.-F. Qiao, W. Shi, J.-B. Wu, D.-S. Jiang, and P.-H. Tan, Phonon and raman scattering of two-dimensional transition metal dichalcogenides from monolayer, multilayer to bulk material, Chem. Soc. Rev. **44**, 2757 (2015).

[28] H. Sahin, S. Tongay, S. Horzum, W. Fan, J. Zhou, J. Li, J. Wu, and F. M. Peeters, Anomalous Raman spectra and thickness-dependent electronic properties of WSe$_2$, Phys. Rev. B **87**, 165409 (2013).

[29] C. M. Chow, H. Yu, A. M. Jones, J. Yan, D. G. Mandrus, T. Taniguchi, K. Watanabe, W. Yao, and X. Xu, Unusual exciton–phonon interactions at van der waals engineered interfaces, Nano Lett. **17**, 1194 (2017).

[30] Rodney Loudon, General space-group selection rules for two-phonon processes, Phys. Rev. **137**, A1784 (1965).

[31] A. A. Mitioglu, S. Anghel, M. V. Ballottin, K. Sushkevich, L. Kulyuk, and P. C. M. Christianen, Anomalous rotation of bright excitons linearly polarized emission from monolayer WSe$_2$ in high magnetic field monolayers (unpublished).

[32] W. Jin, P.-C. Yeh, N. Zaki, D. Zhang, J. T. Liou, J. T. Sadowski, A. Barinov, M. Yablonskikh, J. I. Dadap, P. Sutter, I. P. Herman, and R. M. Osgood, Substrate interactions with suspended and supported monolayer MoS$_2$: Angle-resolved photoemission spectroscopy, Phys. Rev. B **91**, 121409 (2015).

[33] I. Niehues, R. Schmidt, M. Drüppel, P. Marauhn, D. Christiansen, M. Selig, G. Berghäuser, D. Wigger, R. Schneider, L. Braasch, R. Koch, A. Castellanos-Gomez, T. Kuhn, A. Knorr, E. Malic, M. Rohlfing, S. Michaelis de Vasconcellos, and R. Bratschitsch, Strain control of exciton–phonon coupling in atomically thin semiconductors, Nano Lett. **18**, 1751 (2018).

[34] D. Xiao, G.-B. Liu, W. Feng, X. Xu, and W. Yao, Coupled Spin and Valley Physics in Monolayers of MoS$_2$ and Other Group-VI Dichalcogenides, Phys. Rev. Lett. **108**, 196802 (2012).

[35] H. Peelaers and C. G. Van de Walle, Effects of strain on band structure and effective masses in MoS$_2$, Phys. Rev. B **86**, 241401 (2012).

[36] K. S. Novoselov, D. Jiang, F. Schedin, T. J. Booth, V. V. Khotkevich, S. V. Morozov, and A. K. Geim, Two-dimensional atomic crystals, Proc. Natl. Acad. Sci. U.S.A. **102**, 10451 (2005).

[37] G. Wang, L. Bouet, D. Lagarde, M. Vidal, A. Balocchi, T. Amand, X. Marie, and B. Urbaszek, Valley dynamics probed through charged and neutral exciton emission in monolayer WSe$_2$, Phys. Rev. B **90**, 075413 (2014).

[38] T. Smolenski, M. Goryca, M. Koperski, C. Faugeras, T. Kazimierczuk, A. Bogucki, K. Nogajewski, P. Kossacki, and M. Potemski, Tuning Valley Polarization in a WSe$_2$ Monolayer with a Tiny Magnetic Field, Phys. Rev. X **6**, 021024 (2016).

[39] D. Keller, D. R. Yakovlev, G. V. Astakhov, W. Ossau, S. A. Crooker, T. Slobodskyy, A. Waag, G. Schmidt, and L. W. Molenkamp, Magneto-optics of two-dimensional electron gases modified by strong coulomb interactions in ZnSe quantum wells, Phys. Rev. B **72**, 235306 (2005).

[40] A. Granados del Águila, B. Jha, F. Pietra, E. Groeneveld, C. de Mello Donegá, J. C. Maan, D. Vanmaekelbergh, and P. C. M. Christianen, Observation of the Full Exciton and Phonon Fine Structure in CdSe/CdS Dot-in-Rod Heteronanocrystals, ACS Nano **8**, 5921 (2014).

[41] D. R. Yakovlev, V. P. Kochereshko, R. A. Suris, H. Schenk, W. Ossau, A. Waag, G. Landwehr, P. C. M. Christianen, and J. C. Maan, Combined Exciton-Cyclotron Resonance in Quantum Well Structures, Phys. Rev. Lett. **79**, 3974 (1997).

[42] K. Tran, A. Singh, J. Seifert, Y. Wang, K. Hao, J.-K. Huang, L.-J. Li, T. Taniguchi, K. Watanabe, and X. Li, Disorder-dependent valley properties in monolayer WSe$_2$, Phys. Rev. B **96**, 041302 (2017).

[43] Y. Li, J. Ludwig, T. Low, A. Chernikov, X. Cui, G. Arefe, Y. D. Kim, A. M. van der Zande, A. Rigosi, H. M. Hill, S. H. Kim, J. Hone, Z. Li, D. Smirnov, and T. F. Heinz, Valley Splitting and Polarization by the Zeeman Effect in Monolayer MoSe$_2$, Phys. Rev. Lett. **113**, 266804 (2014).

[44] D. MacNeill, C. Heikes, K. F. Mak, Z. Anderson, A. Kormányos, V. Zólyomi, J. Park, and D. C. Ralph, Breaking of Valley Degeneracy by Magnetic Field in Monolayer MoSe$_2$, Phys. Rev. Lett. **114**, 037401 (2015).

[45] H. Rostami, R. Roldán, E. Cappelluti, R. Asgari, and F. Guinea, Theory of strain in single-layer transition metal dichalcogenides, Phys. Rev. B **92**, 195402 (2015).